THE JOURNAL OF PHYSICAL CHEMISTRY B

Article

pubs.acs.org/JPCB

Nitroxide Sensing of a DNA Microenvironment: Mechanistic Insights from EPR Spectroscopy and Molecular Dynamics Simulations

Anna M. Popova,[†,⊥,#] Ma'mon M. Hatmal,[‡,⊥] Maria P. Frushicheva,[†] Eric A. Price,[§,▽] Peter Z. Qin,*[,†] and Ian S. Haworth*[,‡,∥]

[†]Department of Chemistry, University of Southern California, Los Angeles, California 90089-0744, United States

[‡]Department of Biochemistry, University of Southern California, Los Angeles, California 90033-1039, United States

[§]Department of Biological Sciences, University of Southern California, Los Angeles, California 90089-0744, United States

[∥]Department of Pharmacology and Pharmaceutical Sciences, University of Southern California, Los Angeles, California 90089-9121, United States

Supporting Information

ABSTRACT: The behavior of the nitroxide spin labels 1-oxyl-4-bromo-2,2,5,5-tetramethylpyrroline (R5a) and 1-oxyl-2,2,5,5-tetramethylpyrroline (R5) attached at a phosphorothioate-substituted site in a DNA duplex is modulated by the DNA in a site- and stereospecific manner. A better understanding of the mechanisms of R5a/R5 sensing of the DNA microenvironment will enhance our capability to relate information from nitroxide spectra to sequence-dependent properties of DNA. Toward this goal, electron paramagnetic resonance (EPR) spectroscopy and molecular dynamics (MD) simulations were used to investigate R5 and R5a attached as R_p and S_p diastereomers at phosphorothioate $_{pS}C_7$ of d(CTACTG$_{pS}$C$_7$Y$_8$TTAG). d(CTAAAGCAGTAG) (Y = T or U). X-band continuous-wave EPR spectra revealed that the dT$_8$ to dU$_8$ change alters nanosecond rotational motions of R_p-R5a but produces no detectable differences for S_p-R5a, R_p-R5, and S_p-R5. MD simulations were able to qualitatively account for these spectral variations and provide a plausible physical basis for the R5/R5a behavior. The simulations also revealed a correlation between DNA backbone B_I/B_{II} conformations and R5/R5a rotational diffusion, thus suggesting a direct connection between DNA local backbone dynamics and EPR-detectable R5/R5a motion. These results advance our understanding of how a DNA microenvironment influences nitroxide motion and the observed EPR spectra. This may enable use of R5/R5a for a quantitative description of the sequence-dependent properties of large biologically relevant DNA molecules.

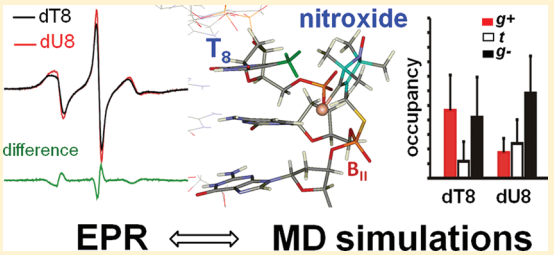

INTRODUCTION

Physical properties of DNA, such as helix geometry, flexibility, water and ion binding, and electrostatics have a critical impact on biological functions of gene expression and regulation. Sequence-dependent deviations from the ideal B form in DNA duplexes play essential roles in DNA recognition by proteins and small molecules.[1−4] For example, DNA sequence-dependent mechanics (i.e., deformability, bending) and local shape variations provide a code to guide nucleosome binding in eukaryotic genomes,[5−7] which may modulate the activity of transcription factors and other DNA-binding proteins and profoundly affect gene expression. However, knowledge of the sequence dependence of the structure and flexibility of DNA has yet to reach a level that allows rational design and manipulation of functions.[2,3] Thus, experimental and computational characterizations of the conformational and dynamic heterogeneity of free DNA duplexes are of significance.[2,4]

Site-directed spin labeling (SDSL) is a biophysical tool for investigating local environments in biomacromolecules.[8−11] In SDSL, a chemically stable nitroxide radical is covalently attached at specific sites of a protein, DNA, or RNA. The nitroxide behavior, which is revealed by electron paramagnetic resonance (EPR) spectroscopy, provides structural and dynamic information on the parent molecule. SDSL requires a small amount of sample (~50 μM in 5 μL) and can be applied to characterize high molecular weight systems under physiological conditions. In nucleic acid studies, SDSL has been used to deduce the structural state of individual nucleotides, to reveal local motions, and to monitor conformational changes in nucleic acids and protein/nucleic acid complexes.[11−17]

We have developed a phosphorothioate labeling scheme[18,19] in which a nitroxide probe (R5 or R5a, Figure 1A) is attached via a flexible R−C−S−P linkage at a R_p or S_p phosphorothioate (Figure 1B) that is chemically substituted at a specific nucleotide in a DNA or RNA strand. R5 and R5a minimally perturb the native duplex conformation of DNA[20−22] and RNA[23,24] and have been used to monitor RNA/RNA interactions,[18] to study motions of an RNA element within a large folded ribozyme,[24] and to measure nanometer distances and

Received: April 6, 2012
Published: May 10, 2012

   dx.doi.org/10.1021/jp303303v | J. Phys. Chem. B 2012, 116, 6387−6396

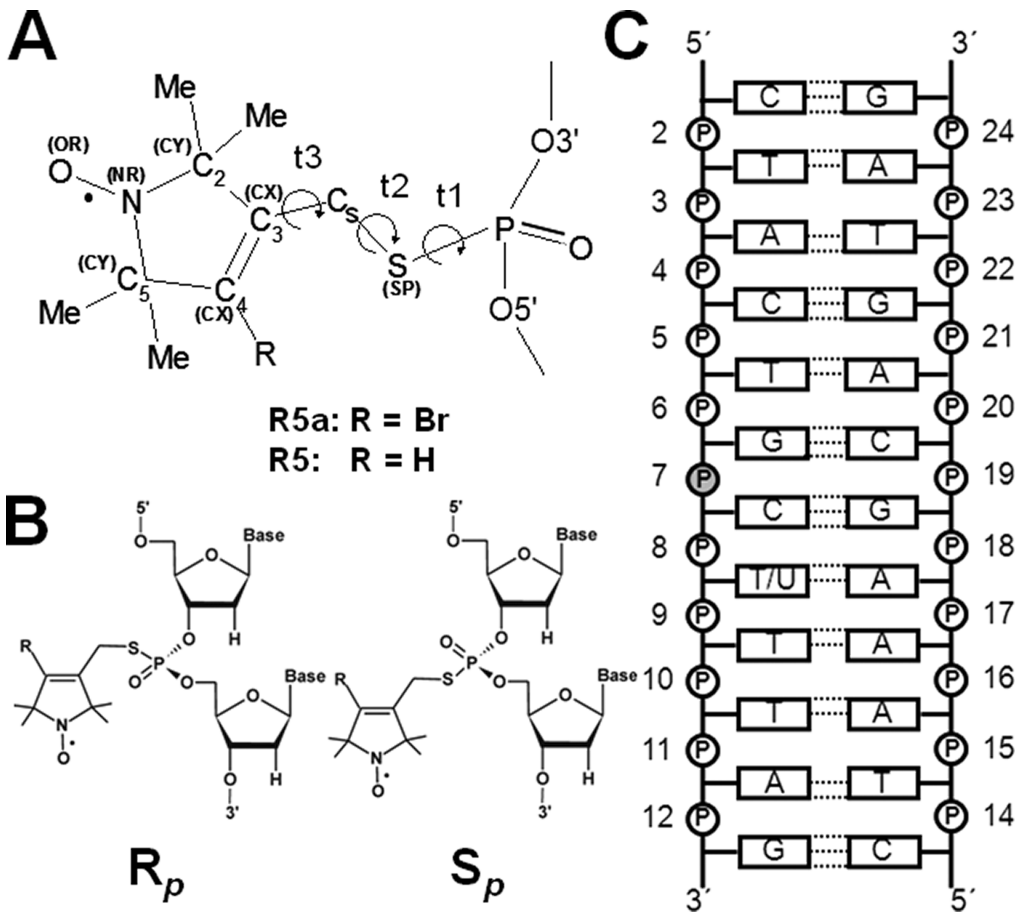

Figure 1. (A) Structure of nitroxide labels (R5, R = H; R5a, R = Br). The torsional angles of the DNA label linker are defined as t1 (O5′−P−S−C_s), t2 (P−S−C_s−C_3), and t3 (S−C_s−C_3−C_2). Symbols in parentheses indicate nonstandard atom types[30] used in the AMBER force field. (B) Absolute R_p and S_p configurations of the labeled phosphorothioate. (C) DNA duplex used in the study. The phosphorothioate-substituted and labeled nucleotide ($_{pS}$C7) is shaded. Nucleotide 8 of the DNA was dT or dU. $_{pS}$C7 was labeled with R5a or R5 as the R_p or S_p diastereoisomer.

conformation in nucleic acids.[20,23,25] We have also shown that X-band continuous-wave (cw) EPR spectra of R5a and R5, which report on nanosecond rotational motions of the nitroxide pyrroline ring, vary within a DNA duplex in a sequence-dependent and stereospecific fashion.[21,22] This indicates that R5a and R5 can act as sensors to reveal sequence-dependent properties of DNA duplexes.

To understand how the local DNA environment governs the rotational behavior of R5a/R5 labels, in this work, we used a combination of EPR spectroscopy and molecular dynamics (MD) simulations to examine how the labels respond to a DNA sequence change, namely, the removal of a methyl group in the major groove of a DNA duplex. The results suggest that specific interactions between the label and the DNA bases, which depend on the conformational preferences of the label and DNA backbone, can modulate rotational motions of the label to an extent detectable by cw-EPR spectroscopy. These results are a key step forward in developing R5 and R5a as spectroscopic probes for examining intrinsic sequence-dependent features in biologically relevant DNA molecules.

MATERIALS AND METHODS

DNA Labeling, Purification, and Diastereomer Separation. The DNA duplexes d(CTACTG$_{pS}$C$_7$T$_8$TTAG)·d(CTAAAGCAGTAG) and d(CTACTG$_{pS}$C$_7$U$_8$TTAG)·d(CTAAAGCAGTAG) ($_{pS}$ = phosphorothioate) were used in the study (Figure 1C). These duplexes are referred to as dT_8 and dU_8, respectively. All DNA oligonucleotides, including those with a phosphorothioate modification, were synthesized by solid-phase chemical synthesis and obtained from Integrated DNA Technologies (Coralville, IA). R5a or R5 was attached to the phosphorothioate-modified DNA strands following reported protocols.[21] The labeled DNA oligonucleotides were purified using anion-exchange HPLC,[21,22,26] which eliminates failed oligonucleotide fragments from DNA synthesis, removes excess spin labels, and separates R_p and S_p phosphorothioate diastereomers. The purities of the labeled R_p and S_p oligonucleotides were determined to be >98% by running anion-exchange HPLC on purified samples.[22] Diastereomer configurations were assigned as reported.[26] The HPLC fractions containing purified labeled DNA were desalted using a G-25 Sephadex column. Desalted oligonucleotides were lyophilized, suspended in 10−15 μL of water, and stored at −20 °C. The final concentration of labeled deoxyoligonucleotides was determined by UV absorption at 260 nm.[21,22]

EPR Spectroscopy. Spin-labeled DNA oligonucleotides were assembled with the complementary strand following a reported protocol.[21,22] The final EPR sample (~10−15 μL) contained 100 mM NaCl, 50 mM Tris-HCl (pH 7.5), 34% (w/w) sucrose, and 20−40 μM labeled DNA duplex. EPR samples were placed in glass capillaries (1.0 mm i.d. × 1.2 mm o.d., Vitrocom, Inc., Mountain Lakes, NJ) that were sealed on one end. cw-EPR spectra were acquired on a X-band Bruker

dx.doi.org/10.1021/jp303303v | J. Phys. Chem. B 2012, 116, 6387−6396

EMX spectrometer equipped with a high-sensitivity cavity (ER 4119HS, Bruker Biospin, Inc., Billerica, MA) using a 2 mW incident microwave power and a field modulation of 1−2 G at 100 kHz. The sample temperature was maintained at 25 °C using a liquid nitrogen variable temperature control setup. All EPR spectra were baseline corrected and normalized to the same number of spins using software kindly provided by the Hubbell group at UCLA. In some cases, EPR spectra revealed features from a residual amount of a detached spin probe (<3%). These features were manually subtracted from the reported spectra.[21,22]

EPR Spectra Fitting. Spectral fitting was carried out as previously described[22] using a MATLAB-based EPRLL program suite[27] that implements the microscopic order macroscopic disorder (MOMD) model.[28] The $\boldsymbol{g}$ and $\boldsymbol{A}$ tensor, the diffusion tilt angle, the number of director orientations, and dimensions of the basis set were fixed at previously reported values.[22] Variable fitting parameters (Table S1 in the Supporting Information) included the following: (i) $\bar{R}$ and N, spherical components of the rotational diffusion rate tensor [$\bar{R} = (R_\perp^2 \cdot R_\parallel)^{1/3}$ and $N = R_\parallel/R_\perp$, where $R_\parallel$ and $R_\perp$ are the respective rate constants for rotations parallel and perpendicular to the nitroxide principal diffusion axis]; (ii) c_{20}, the coefficient of an ordering potential [$U(\theta) = -1/2(k_bT)\cdot c_{20}\cdot(3\cos^2\theta - 1)$, where θ is an instantaneous angle relating the director to the nitroxide diffusion frame]; and (iii) $\Delta^{(0)}$, the Gaussian inhomogeneous broadening factor. From the ordering potential, an order parameter, S_{20}, was computed as $S_{20} = \langle(3\cos^2\theta - 1)/2\rangle = \{[\int 1/2(3\cos^2\theta - 1)\cdot\exp(-U(\theta)/k_bT)\cdot\sin(\theta)\, d\theta]/[\int \exp(-U(\theta)/k_bT)\cdot\sin(\theta)\, d\theta]\}$. Errors for the fitting parameters were obtained as previously described.[22]

Structure Building for MD Simulations. Input structures for the MD simulations were built from the NMR structure of the dT_8 duplex (model 1 of 1CS2.PDB),[29] with either R5a or R5 added using the NASNOX algorithm.[19,30] In this procedure, a nonbridging oxygen atom of the phosphodiester of nucleotide 7 (OA and OB for the S_p and R_p diastereoisomers, respectively) was substituted by a sulfur atom with a P−S bond of 1.99 Å, but otherwise, the experimental geometry of the duplex was retained. Eight structures were built for each combination of label (R5 or R5a), chirality (R_p or S_p), and DNA sequence (dT_8 or dU_8) with the label conformation set at t1 = t2 = t3 = 180° (see Figure 1A for the definition of torsional angles t1, t2, and t3). Two more sets of eight structures each were built with starting conformations of t1 = 60° (S_p) or −60° (R_p), t2 = 180°, and t3 = 0°; and t1 = 60° (S_p) or −60° (R_p), t2 = 180°, and t3 = 120°. Overall, 24 structures were used as starting points for MD simulations of 10 ns each. On the basis of the results of these simulations, a fourth set with t1 = 180°, t2 = 120°, and t3 = 180° was used for additional simulation of selected combinations of the chirality, label, and DNA sequence.

Parameters for the 1-Oxyl-4-bromo-2,2,5,5-tetramethylpyrroline (R5a) Label. A previously defined geometry for the R5 label[30] was maintained for R5a, and the Br atom was added to position 4 of the pyrroline ring with a bond length of 1.94 Å (see Figure 1A for atom nomenclature). Further parametrizations were based on those for the "br" atom type in the General AMBER ForceField (GAFF):[31] CX−br bond k_{str} = 269.6 kcal/(mol·Å^2), r_{eq} = 1.897 Å (based on GAFF CA−br); CX−CX−br and CY−CX−br angles k_θ = 63.0 kcal/(mol·rad^2), θ_0 = 123.55° (force constant from GAFF, geometry from Price et al.[30]). Atomic point charges (mE) for the R5a label were P, +601; O5′, −327; O3′, −327; O, −344; S, −129; CS (HS), +33 (+57); C2, +58; C3, −54; N1, +84; C4, +34; Br, −87; C5, +74; O1, −345; C2-Me (H-Me), −88 (+46); and C5-Me (H-Me), −83 (+46).

MD Simulations. Each labeled duplex was solvated in a periodic box of TIP3P water molecules with the box extending 12 Å from the extremes of the solute in the ±x-, ±y-, and ±z-directions. This gave a box of approximate dimensions 60 × 60 × 75 Å^3 that contained 6000−6500 water molecules (the exact number depended on the starting structure for the simulation). The labeled duplexes were neutralized by addition of 21 sodium ions, and the system was minimized for 1000 steps (500 steps of steepest decent, followed by 500 steps of conjugate gradient minimization). Simulations were run using the AMBER parm99 force field with a time step of 0.002 ps, a residue-based cutoff of 8 Å, and the particle-mesh Ewald method for electrostatic interactions.[32] SHAKE was applied to all hydrogen atoms, and the target pressure was 1 atm. Equilibration of the solvent molecules was achieved in an initial simulation of 5000 steps (100 ps) with position restraint of all solute atoms (except for sodium ions) with a force constant of 20 kcal/(mol Å^2), during which the temperature of the system was raised linearly from 0 to 298 K over the first 2500 steps (50 ps). Following the 100 ps solute-restrained period, the restraint on the solute atoms was removed, and a further 100 ps of equilibration was performed at 298 K. This was followed by a 10 ns simulation for data collection, during which structures were collected every 0.1 ps.

Three simulations of 10 ns each were also performed for the unlabeled DNA duplex, starting from PDB ID 1CS2 (model 1) and using an identical solvation and equilibration procedure to that for the labeled duplexes. For the unlabeled helix, the structure after 10 ns was resolvated and subjected to re-equilibration to generate a second 10 ns trajectory. The structure after 20 ns was used similarly as a starting point for the third simulation. Results from all simulations were visualized using WebLab Viewer (Molecular Simulations Inc., San Diego, CA), and geometrical data were obtained using AMBER (PTRAJ) and CURVES 5.2.[33]

RESULTS

EPR Spectra Reveal That the dT_8 to dU_8 Change Affects Rotational Motion of R_p-R5a Only. In this work, R5a and R5 were attached to nucleotide 7 located at the center of the dT_8 or dU_8 duplex (Figure 1C), and R_p and S_p diastereomers were separated to >98% pure (see the Materials and Methods). R5a or R5 labeling previously has been shown to minimally perturb the native B-DNA conformation of the dT_8 duplex.[20−22] The dU_8 duplex, which differs from dT_8 only by a thymine C5-methyl group residing in the DNA major groove, is expected to maintain a B form conformation with or without R5/R5a attachment. This is indeed the case observed in MD simulations.

Figure 2 shows EPR spectra of R5a and R5 obtained at 25 °C. The dT_8 to dU_8 change results in a small but reproducible change in R_p-R5a spectra. The R_p-R5a-dU_8 spectrum has narrower lines as compared to that of R_p-R5a-dT_8, indicating an increase in R5a mobility upon removal of the dT_8 C5-methyl group. No detectable spectral differences were observed for S_p-R5a, R_p-R5, and S_p-R5 (Figure 2), which suggests that changing dT_8 to dU_8 has no measurable effect on nanosecond rotations of these probes. We also note that the R_p-R5 spectra are broader than those of S_p-R5 (Figure 2). This is consistent with previously reported R_p-R5a and S_p-R5a behavior,[22] which has been attributed to the R_p-diastereomer

dx.doi.org/10.1021/jp303303v | J. Phys. Chem. B 2012, 116, 6387−6396

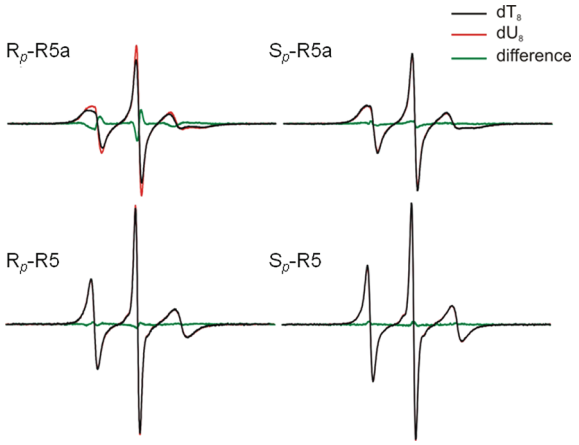

Figure 2. EPR spectra obtained at 25 °C. Black lines represent spectra obtained in the d(CTACTG$_{pS}$C$_7$T$_8$TTAG)·d(CTAAAGCAGTAG) duplexes (dT$_8$), and red lines represent those in the d-(CTACTG$_{pS}$C$_7$U$_8$TTAG)·d(CTAAAGCAGTAG) duplexes (dU$_8$). Green lines represent the corresponding difference spectra.

positioning the nitroxide toward the major groove of the DNA duplex, while the S_p-diastereomer positions the nitroxide toward the solvent.

To further characterize rotational motions of R5a, spectral simulations were carried out using the MOMD model, which describes the nitroxide motion within the macromolecular environment as an anisotropic rotational diffusion constricted by an ordering potential.[27] Simulations yield two key parameters: (i) $\bar{R}$, which describes the rate of nitroxide rotational motions, and (ii) S_{20}, which provides a measure of local ordering. The simulations gave best-fit spectra that match the corresponding measured spectra very well (Figure 3A). The dT$_8$ to dU$_8$ change was found to increase R_p-R5a mobility, with a faster rate (larger $\bar{R}$) and lower ordering (smaller S_{20}) obtained for R_p-R5a-dT$_8$ (Figure 3B). For S_p-R5a, neither rate nor order parameters are affected by the change from dT$_8$ to dU$_8$ (Figure 3B). This is in complete agreement with conclusions drawn from direct line shape comparisons described above.

In summary, EPR spectra reveal that the dT$_8$ to dU$_8$ change gives rise to increased mobility for R_p-R5a but has no detectable effects on S_p-R5a, R_p-R5, and S_p-R5. These observations are accounted for by MD simulations described below.

MD Simulations Qualitatively Capture Observed Features of Nitroxide Rotational Behavior in Response to the dT$_8$ to dU$_8$ Change. A total of 40 simulations of 10 ns each were performed in explicit solvent using AMBER on the dT$_8$ and dU$_8$ duplexes carrying R5a or R5 as the R_p or S_p

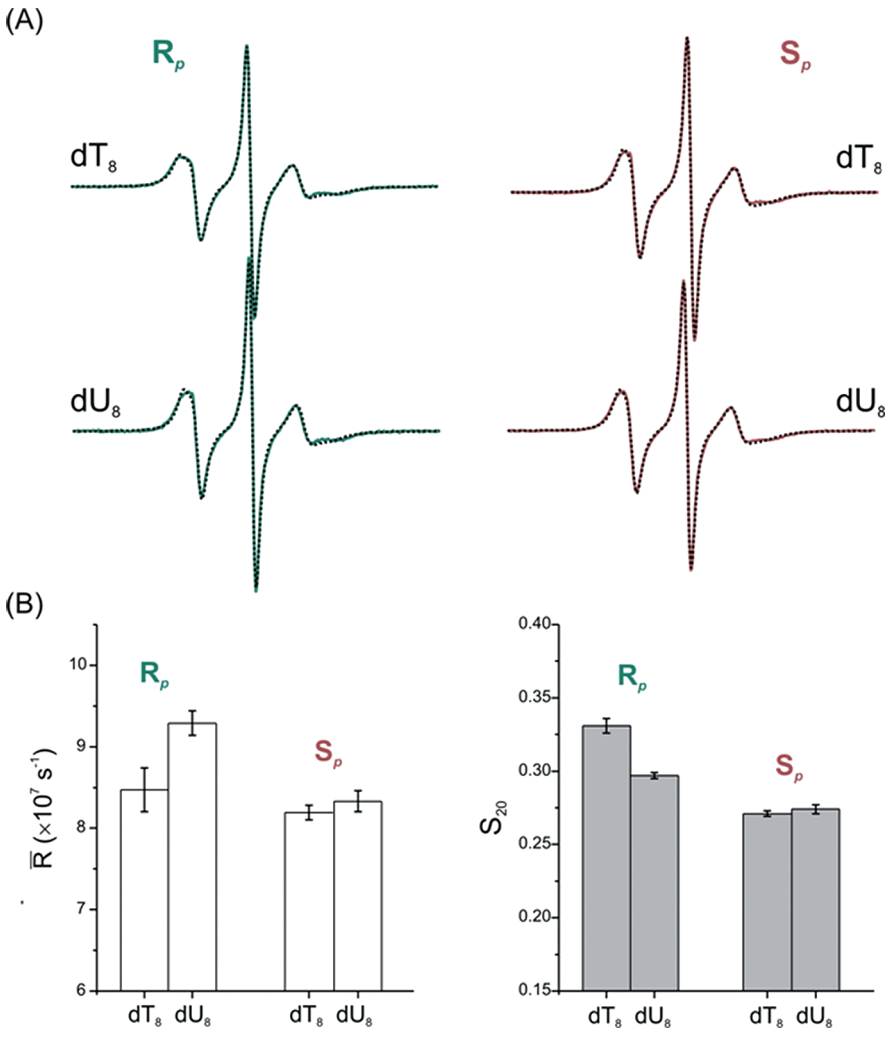

Figure 3. R5a spectral simulations. (A) Overlays of measured (solid lines) and simulated (dotted lines) spectra. (B) Comparisons of nitroxide motional parameters obtained from simulations. Additional details on simulation parameters are given in Table S1 in the Supporting Information.

dx.doi.org/10.1021/jp303303v | J. Phys. Chem. B 2012, 116, 6387−6396

Table 1. Label Conformer Distributions in MD Simulations of DNA Duplexes of Sequence d(CTACTG$_{pS}$C$_7$Y$_8$TTAG)·d(CTAAAGCAGTAG) (Y = T or U) Labeled with a R5a or a 1-Oxyl-2,2,5,5-tetramethylpyrroline (R5) Radical at $_{pS}$dC$_7$

				t1 (%)[b,c]			t2 (%)[b,c]			t3 (%)[b,d]	
label	chirality	dY$_8$	n[a]	g+	t	g−	g+	t	g−	+100°	−100°
R5a	R$_p$	dT$_8$	8	46.6 ± 24.3	11.6 ± 13.5	41.8 ± 27.7	0.5 ± 0.7	98.9 ± 2.3	0.6 ± 1.8	64.4 ± 39.6	35.6 ± 39.6
R5a	R$_p$	dU$_8$	6	17.7 ± 9.7	23.9 ± 16.3	58.4 ± 25.4	2.9 ± 4.4	93.6 ± 6.0	3.5 ± 4.1	57.5 ± 33.7	42.5 ± 33.7
R5	R$_p$	dT$_8$	3	18.5 ± 4.9	23.8 ± 9.5	57.6 ± 13.0	8.8 ± 6.5	72.7 ± 5.7	18.5 ± 1.0	52.8 ± 7.9	47.2 ± 7.9
R5	R$_p$	dU$_8$	3	14.2 ± 8.8	16.8 ± 9.7	68.9 ± 4.8	13.3 ± 6.9	67.0 ± 17.1	19.7 ± 21.6	51.3 ± 10.1	48.7 ± 10.1
R5a	S$_p$	dT$_8$	8	48.6 ± 9.7	48.7 ± 9.3	2.6 ± 1.4	5.8 ± 4.7	88.7 ± 8.2	5.5 ± 7.0	69.1 ± 35.8	31.1 ± 35.9
R5a	S$_p$	dU$_8$	6	37.0 ± 14.2	59.0 ± 14.9	3.9 ± 2.1	4.9 ± 7.9	91.0 ± 7.2	4.2 ± 4.6	60.1 ± 35.5	39.9 ± 35.5
R5	S$_p$	dT$_8$	3	52.7 ± 19.5	45.3 ± 18.2	2.0 ± 1.7	21.2 ± 9.3	59.7 ± 3.7	19.1 ± 12.6	46.3 ± 20.6	53.7 ± 20.6
R5	S$_p$	dU$_8$	3	38.8 ± 18.2	58.8 ± 17.3	2.4 ± 1.3	8.9 ± 4.7	58.0 ± 5.6	33.1 ± 8.9	54.0 ± 6.9	46.0 ± 6.9

[a]Number of simulations of 10 ns each. [b]Torsion angles are defined in Figure 1A. Average and standard deviations are calculated from the corresponding individual 10 ns simulations. [c]g+, 0−120°; t, 120−240°; and g−, 240−360°. [d]Torsion angle t3 adopts values centered on +100 and −100°. Each distribution was determined based on conformations with t3 > 0° and t3 < 0°, respectively, for a torsional angle range from +180 to −180°.

phosphorothioate diastereomer of nucleotide 7 (Figure 1). For each sample set, defined by diastereomer configuration (R$_p$ or S$_p$), label identity (R5a or R5), and DNA sequence (dT$_8$ or dU$_8$), the results were obtained by analyzing multiple simulations that differed only in the starting conformation of the label, defined by torsion angles t1, t2 and t3 around bonds connecting the nitroxide pyrroline ring to the DNA (Figure 1A). Details of the simulations are reported in Tables S2 and S3 in the Supporting Information for R$_p$ and S$_p$ labels, respectively. In each simulation, the energy of the system was stable, and the DNA duplex structure was retained, as confirmed by analysis of helical parameters and base pair hydrogen bonds (data not shown).

Variations of the t1, t2, and t3 torsion angles reflect rotational motions of the nitroxide with respect to the DNA, which is measured by the cw-EPR spectra described above. Torsion angle distributions from all simulations are summarized in Table 1 (see also Tables S2 and S3 in the Supporting Information). For the R$_p$ labels, the MD data show that the dT$_8$ to dU$_8$ change yields significant changes only for R$_p$-R5a, with occupancy of the t1 *gauche*+ (g+) conformer being 46.6 ± 24.3% for R$_p$-R5a-dT$_8$ versus 17.7 ± 9.7% for R$_p$-R5a-dU$_8$ (Tables 1 and S2 in the Supporting Information). This suggests that the dT$_8$ to dU$_8$ change alters the rotational behavior of R$_p$-R5a but has no apparent effect on R$_p$-R5. This is in agreement with the EPR data (Figures 2 and 3).

For the S$_p$ labels, the sequence change from dT$_8$ to dU$_8$ results in no significant changes of all torsion angle distributions except for t2 in S$_p$-R5, in which the average occupancy of g+ and *gauche*− (g−) conformers differ beyond one standard deviation (Tables 1 and S3 in the Supporting Information). Examination of MD data for S$_p$ labels revealed no discernible nitroxide/DNA interaction that is dependent on the dT$_8$ to dU$_8$ change, since the S$_p$ labels are directed away from the DNA helix and into the solvent.[22,30] This is consistent with the absence of a difference between the spectra of the S$_p$ labels (Figure 2).

In the following text, only the MD data for the R$_p$ labels are further analyzed to explore the physical basis for the two key features observed in the EPR spectra: (i) the difference between R$_p$-R5a-dT$_8$ and R$_p$-R5a-dU$_8$ and (ii) the lack of a detectable difference between R$_p$-R5-dT$_8$ and R$_p$-R5-dU$_8$.

R$_p$-R5a and R$_p$-R5 Show Different t2 and t3 Rotational Behavior. Representative traces for torsion angles t1, t2, and t3 for R$_p$-R5a-dT$_8$ and R$_p$-R5-dT$_8$ are shown in Figure 4. A clear feature of R$_p$-R5a-dT$_8$ is that motions at t2 and t3 are limited on the nanosecond time scale. Throughout all simulations, including the one with the nitroxide starting conformation deliberately set at t2 = 120°, t2 was fixed in the *trans* (t) conformation (Figure 4B, Tables 1 and S2 in the Supporting Information). In comparison, t2 for R$_p$-R5-dT$_8$ also favors a t conformation (Figure 4E, Tables 1 and S2 in the Supporting Information), but deviations from t occur on the nanosecond time scale. Clearly, the Br atom in R5a is restricting this motion.

For t3, the trace of R$_p$-R5a-dT$_8$ in Figure 4C shows persistence of a conformation around +100°. However, analysis of all data for R$_p$-R5a-dT$_8$ (Tables 1 and S2 in the Supporting Information) shows that t3 adopts two conformations centered around +100 and −100° (+260°), respectively, with infrequent transitions between these two positions. Among the eight 10 ns R$_p$-R5a-dT$_8$ simulations, four had no formal t3 transition, and four gave only one transition (data not shown). In these two conformations, the pyrroline ring of R5a is positioned at the same location, but the peripheral functional groups (i.e., 4-Br, C2, and C5 methyls) are oriented differently with respect to the DNA. Over all R$_p$-R5a-dT$_8$ simulations, occupancy of the two t3 conformations is approximately equal (Table 1). Similar +100 and −100° conformations are seen for R$_p$-R5-dT$_8$ but with more frequent transitions between them (Figure 4F). The additional motion may reflect the greater mobility of t2, although there is no clear correlation between the t2 and the t3 torsional angles for R$_p$-R5-dT$_8$ (Figure 4E,F).

The characteristics of t2 and t3 described for R5 and R5a occurred in all simulations regardless of diastereomeric configuration (R$_p$ and S$_p$) and DNA sequence (dT$_8$ and dU$_8$) (Table 1). Therefore, they appear to be inherent properties of the respective labels. The MD results show that the presence of the 4-Br group limits rotations about bonds connecting the pyrroline ring to the DNA. The t2 and t3 motions in R$_p$ labels are similar for the dT$_8$ and dU$_8$ duplexes (Table 1), but limitations on t2 and t3 reduce the available conformations of R$_p$-R5a. This is an important factor in accounting for the sequence-dependent EPR spectral changes observed for R$_p$-R5a but not for R$_p$-R5 (see the following).

Interactions between R$_p$-R5a and DNA Account for Sequence-Dependent Changes in EPR Spectra. For R$_p$-R5a, the t1 torsion samples the canonical g+, t, and g− conformations (Figure 4A), with the dT$_8$ to dU$_8$ change significantly decreasing the t1 g+ occupancy (Table 1). Examples of R$_p$-R5a-dT$_8$ t1 g+ conformations with t3 = +100 or −100° are shown in Figure 5A,B, respectively. In both conformations, the nitroxide pyrroline ring is proximal to the dT$_8$ C5-methyl

dx.doi.org/10.1021/jp303303v | J. Phys. Chem. B 2012, 116, 6387−6396

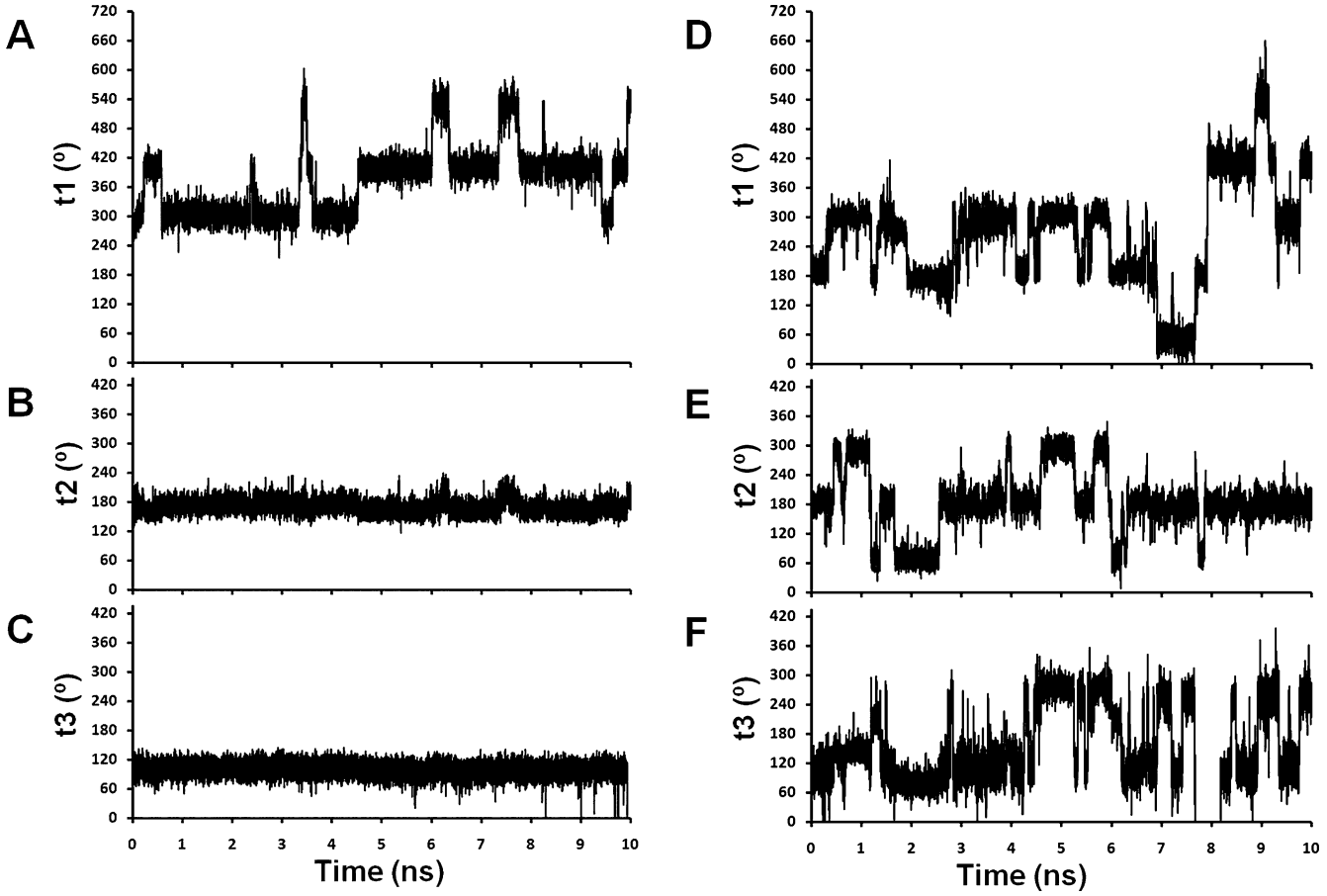

Figure 4. Sample traces of torsional motions for R_p-R5a-dT_8 (A, t1; B, t2; C, t3; simulation #1) and R_p-R5-dT_8 (D, t1; E, t2; F, t3; simulation #13). The t1 traces (A, D) are shown over a range of 0−720° with occupancy of *g*+ (60 or 420°), *t* (180 or 540°), and *g*− (300 or 660°). In F, the trace between 7.5 and 8.5 ns reflects t3 motion from +260° through a 360° turn to −100° (an equivalent conformation with a numerical value off the scale of the *y*-axis) and then a reverse 360° turn back to +260°, with only brief occupancy of the +100° conformer during each full turn.

group in a face-on position, suggesting a direct interaction between these two entities. We also note that in Figure 5A,B the $dG_{6\text{-}pS}dC_7$ dinucleotide linkage adopts a B_{II} conformation (defined as ε/ζ: *g*−/*t*; ε-ζ ∼ +90°),[34] whereas all simulations started with $dG_{6\text{-}pS}dC_7$ in a B_I conformation (ε/ζ: *t*/*g*−; ε-ζ ∼ −90°).[34] The relationship between the nitroxide t1 torsion and the $dG_{6\text{-}pS}dC_7$ dinucleotide conformation will be further examined later.

The characteristics of the conformers shown in Figure 5A,B are maintained for the entire R_p-R5a-dT_8 t1 *g*+ ensemble. Specifically, distributions of distances between the dT_8 C5-methyl group and center of the pyrroline ring, the peripheral methyl groups of the ring, and the 4-Br atom each show predominantly one population, with an average distance of ≤5.1 Å in each case (Table 2). These close contacts suggest the presence of a hydrophobic interaction between the label and the dT_8 C5-methyl group, which may explain the higher t1 *g*+ occupancy for R_p-R5a-dT_8 as compared to R_p-R5a-dU_8.

The t1 *g*− is another significantly occupied conformer for R_p-R5a (Table 1 and Figure 5C). In this conformer, the pyrroline ring is moved away from the dT_8 C5-methyl group (compare Figure 5A,C), with the average distance between the center of the pyrroline ring and dT_8 C5-methyl becoming 6−8 Å (Table 2). At the same time, an average distance of <5.0 Å from the dT_8 C5-methyl to the R5a peripheral methyl groups or 4-Br atom is observed in three of the four ensembles of t1 *g*− conformers (Table 2), as well as in one of the subpopulations of the fourth ensemble (*g*−, *t*, −100; B_{II}) (Table S4 in the Supporting Information). This indicates that R_p-R5a t1 *g*- conformers may also support interactions between the label and the dT_8 C5-methyl. A similar conclusion can be drawn regarding the t1 *t* conformers (Table S4 in the Supporting Information).

Overall, upon analysis of all R_p-R5a-dT_8 MD simulations, 86.8% of the conformer population was found to have one or more contacts of <5.0 Å between the dT_8 C5-methyl group and the center of the R_p-R5a pyrroline, a ring methyl group, or the 4-Br atom. This suggests that a majority of the population may support direct interaction between the dT_8 C5-methyl group and the R_p-R5a. The dT_8 to dU_8 change abolishes this specific label/DNA interaction, thus resulting in the mobility changes observed in the EPR spectra of R_p-R5a-dT_8 and R_p-R5a-dU_8 (Figures 2 and 3).

Analysis of R_p-R5 Sequence-Dependent Behavior. MD data reveal both similarities and differences between R_p-R5 and R_p-R5a. All major conformers of R_p-R5a are also present for R_p-R5 and maintain similar characteristics, as judged by the distances from the dT_8 C5-methyl to the pyrroline ring center and methyl groups (Tables 2 and S4 and S5 in the Supporting Information). This suggests that interaction between the label and the dT_8 C5-methyl may occur for certain R_p-R5 conformers (e.g., t1 *g*+). However, contrary to R5a, R5 shows frequent transitions between t3 +100 and −100° (Figure 4F), as well as t2 transitions among *g*+, *t*, and *g*− (Figure 4E). Consequently, R_p-R5 can access many more sterically allowed conformations

dx.doi.org/10.1021/jp303303v | J. Phys. Chem. B 2012, 116, 6387−6396

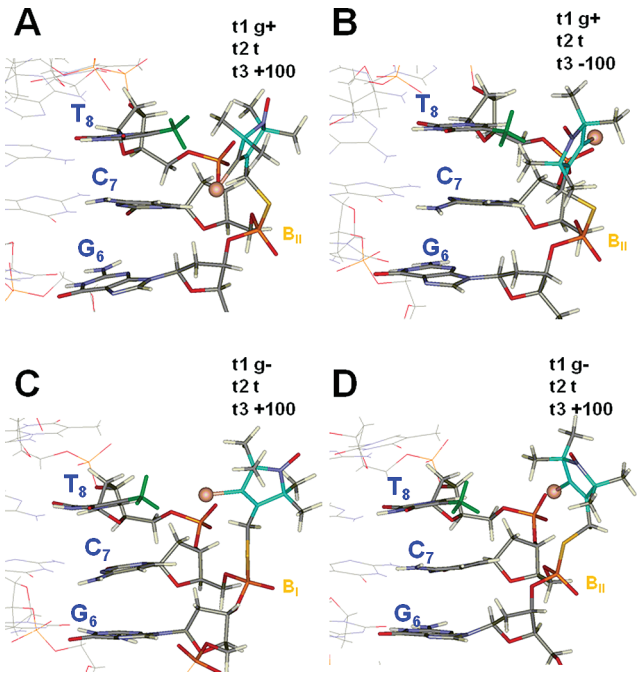

Figure 5. Representative structures from simulations of R_p-R5a-dT_8. (A) t1 *g*+, t2 *t*, t3 +100°, $dG_{6\text{-}pS}dC_7$ B_{II} (simulation #1, at 5 ns, see Figure 4A–C). (B) t1 *g*+, t2 *t*, t3 −100°, $dG_{6\text{-}pS}dC_7$ B_{II} (#37, at 8 ns). (C) t1 *g*−, t2 *t*, t3 +100°, $dG_{6\text{-}pS}dC_7$ B_I (#1, at 2 ns, see Figure 4A–C). (D) t1 *g*−, t2 *t*, t3 +100°, $dG_{6\text{-}pS}dC_7$ B_{II} (#27, at 3.8 ns, see Figure 6). In each structure, the dT_8 methyl group is colored green, the C atoms of the pyrroline ring are colored light blue, and the bromine atom is shown as a brown sphere. The backbone conformation for the $dG_{6\text{-}pS}dC_7$ dinucleotide (B_I or B_{II}) is shown in orange.

as compared to R_p-R5a, and many of them may not have interactions between the dT_8 C5-methyl and the label (Tables 2 and S5 in the Supporting Information). For example, in (t1 *g*−; t2 *g*−) conformers, which are largely absent in R_p-R5a but account for ∼ 18% of the total R_p-R5 population (Table 2), the pyrroline ring center and methyl groups are on average >7.5 Å away from dT_8 C5-methyl (Table 2). These conformers are unlikely to be involved in direct interactions between the label and the DNA. Furthermore, instead of a 4-Br atom, R5 has a 4-H (Figure 1A), which is unable to interact with dT_8 C5-methyl.

Overall, analyses of all R_p-R5-dT_8 MD simulations reveal that 40.1% of the label conformers have at least one distance <5.0 Å from the dT_8 C5-methyl group to the pyrroline ring center or a ring methyl group. This is more than a 2-fold reduction as compared to R_p-R5a. Therefore, it is likely that R_p-R5 shows no detectable sequence-dependent spectral changes because its sensitivity to the presence of the dT_8 C5-methyl is reduced by a combination of two factors: (i) fewer label functional groups making direct interactions with dT_8 C5-methyl and (ii) a smaller fraction of conformers that include these interactions. Both of these changes originate from removal of the 4-Br atom.

Correlation of t1 and DNA Backbone Conformations for R_p Labels. An intriguing feature observed for R_p labels was the apparent dependence of the t1 value on the DNA backbone conformation at the $dG_{6\text{-}pS}dC_7$ dinucleotide (Figure 5 and Table 2). This behavior is further illustrated in Figure 6 using one of the R_p-R5a-dT_8 simulations (simulation #27, Table S2 in the Supporting Information). The t1 torsion angle shows a similar distribution to that in Figure 4A, with approximately half occupancy of *g*+ and *g*− conformations (420 and 300°, respectively, in Figure 6A). Notably, the t1 *g*+ can only form when $dG_{6\text{-}pS}dC_7$ adopts a B_{II} conformation (Figure 6B,C). The strict association of t1 *g*+ with $dG_{6\text{-}pS}dC_7$ B_{II} is true for both R_p-R5a and R_p-R5, since the total occupancies of t1 *g*+; $dG_{6\text{-}pS}dC_7$ B_I for R_p-R5a-dT_8 and R_p-R5-dT_8 were only 0.02 and 0.07%, respectively, over all simulations (Tables 2 and S4 and S5 and Figure S1 in the Supporting Information). Modeling showed that for a R_p label, the t1 *g*+ conformer has severe clashes of the pyrroline ring with the dG_6 sugar when $dG_{6\text{-}pS}dC_7$ remains in the B_I conformation, thus explaining the necessity of adopting the B_{II} conformation.

A control 30 ns MD simulation of the unlabeled dT_8 duplex gave a 35.3%:63.7% ratio for the B_I:B_{II} equilibrium at dG_6-dC_7 (Table S6 and Figure S2 in the Supporting Information). A similar B_I:B_{II} ratio was found upon analyzing all R_p-R5a-dT_8 and R_p-R5-dT_8 simulations (38.0%:61.8% and 40.9%:58.3%, respectively, Table S6 in the Supporting Information). This

Table 2. Distances from the 5-Methyl Carbon Atom of dT_8 to R_p-R5a and R_p-R5 Labels in Key Conformers Found in Simulations of the Labeled DNA Duplex d(CTACT$G_{pS}C_7T_8$TTAG)·d(CTAAAGCAGTAG)[a]

conformer[b] (t1, t2, t3)	DNA[c]	R5a occupancy (%)	R5a[d] pyrroline ring center (Å)	R5a[d] closest ring methyl (Å)	R5a[d] ring 4-Br (Å)	R5 occupancy (%)	R5[d] pyrroline ring center (Å)	R5[d] closest ring methyl (Å)
g+, *t*, +100	B_I	0.0[e]				0.0[e]		
g+, *t*, −100	B_I	0.0[e]				0.0[e]		
g+, *t*, +100	B_{II}	32.9	4.9 ± 0.5	4.1 ± 0.5	4.9 ± 0.9	8.8	5.4 ± 0.7	4.0 ± 0.5
g+, *t*, −100	B_{II}	13.6	5.1 ± 0.7	4.3 ± 0.6	5.0 ± 1.2	9.2	5.3 ± 0.7	4.2 ± 0.6
g−, *t*, +100	B_I	27.9	6.6 ± 0.8	5.8 ± 0.9	4.2 ± 0.5	9.6[f]	6.9 ± 1.6	6.1 ± 1.9
g−, *t*, −100	B_I	8.3	6.3 ± 0.8	4.1 ± 0.8	8.9 ± 0.7	16.1	6.4 ± 0.9	4.2 ± 1.0
g−, *t*, +100	B_{II}	1.7	7.0 ± 0.8	6.4 ± 1.0	4.4 ± 0.8	6.6[f]	8.4 ± 1.3	8.1 ± 1.5
g−, *t*, −100	B_{II}	3.1[f]	8.1 ± 1.4	6.0 ± 1.6	9.6 ± 1.1	5.0[f]	7.7 ± 1.5	5.7 ± 1.7
g−, *g*−, +100	B_I	0.0[e]				2.8[f]	8.9 ± 1.4	7.5 ± 1.6
g−, *g*−, −100	B_I	0.2	9.3 ± 1.0	9.4 ± 1.2	7.8 ± 0.9	2.9[f]	8.3 ± 1.3	8.1 ± 1.5
g−, *g*−, +100	B_{II}	0.0[e]				10.0	9.7 ± 0.7	9.1 ± 0.8
g−, *g*−, −100	B_{II}	0.4	9.4 ± 0.8	9.0 ± 0.9	8.8 ± 0.8	2.5	9.4 ± 0.9	9.4 ± 1.0

[a]Analyses carried out on 400000 R_p-R5a-dT_8 structures (eight 10 ns simulations) and 150000 R_p-R5-dT_8 structures (three 10 ns simulations). Data for all conformers are shown in Tables S4 (R5a) and S5 (R5) in the Supporting Information. [b]*g*+, 0–120°; *t*, 120–240°; and *g*−, 240–360°. [c]Backbone conformation at the $dG_{6\text{-}pS}dC_7$ dinucleotide (see Table S6 in the Supporting Information). [d]Average ± standard deviation of distance (Å) determined for the corresponding ensemble of conformers. [e]Occupancy ranges from 0 to 0.03% [see Tables S4 (R5a) and S5 (R5) in the Supporting Information]. [f]Bimodal distributions observed [see Tables S4 (R5a) and S5 (R5) in the Supporting Information].

dx.doi.org/10.1021/jp303303v | J. Phys. Chem. B 2012, 116, 6387–6396

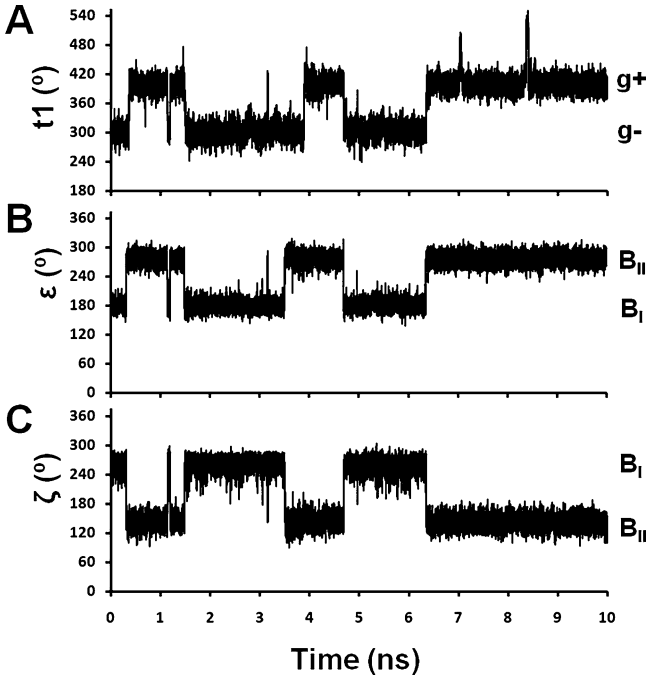

Figure 6. Sample traces of torsional motions for R_p-R5a-dT_8 (simulation #27). (A) t1. (B) ε torsion angle of dG_6: *t* conformers correspond to the B_I conformation at $dG_{6\text{-}pS}dC_7$ and *g*− conformers to B_{II}. (C) ζ torsion angle of dG_6: *g*− conformers correspond to the B_I conformation and approximately *t* conformers to B_{II}. See Table S6 in the Supporting Information for a detailed definition of B_I and B_{II} conformations.

suggests that interactions between the R_p labels and the DNA are not strong enough to alter the thermodynamics of the B_I:B_{II} equilibrium. In addition, analysis of R_p-R5a-dU_8 traces shows approximately 52% B_{II} occupancy, indicating that the nucleotide at position 8 does not significantly influence B_I/B_{II} equilibrium at $dG_{6\text{-}pS}dC_7$. Close examination of the MD traces shows that the t1 *g*+ conformation does not induce the $dG_{6\text{-}pS}dC_7$ B_{II} conformation but rather forms after a B_I to B_{II} transition at $dG_{6\text{-}pS}dC_7$. For example, the t1 *g*− to *g*+ transition between 3 and 4 ns in Figure 6A clearly occurs after a B_I to B_{II} transition at $dG_{6\text{-}pS}dC_7$ (Figure 6B,C), and the intermediate structure (i.e., t1 *g*−; $dG_{6pS}dC_7$ B_{II}) is formed (Figure 5D).

Previously, MD simulations have observed that B_I/B_{II} transitions occur in nanosecond time scale.[34−37] Both MD simulation[36] and NMR measurements[37] have shown that a G_pC dinucleotide step, at which the R5/R5a labels were attached in this study, have a significant population of the B_{II} conformation. Overall, our results indicate that the R_p labels are exploring a naturally occurring transition of the DNA backbone to establish (additional) contact(s) between the dT_8 C5-methyl group and the pyrroline ring, which subsequently influences nitroxide motions and gives rise to the observed cw-EPR spectral changes. This suggests a direct connection between label motion and local DNA backbone dynamics.

DISCUSSION

Synergistic Combination of EPR and MD Simulation for Probing DNA Local Environment Using Spin Labeling. In this work, the behavior of R5 and R5a nitroxide labels in response to a subtle DNA sequence change was examined using a combination of EPR spectroscopy and MD simulation. X-band cw-EPR spectra of labeled DNA duplexes revealed that a dT_8 to dU_8 change altered the nanosecond rotational motions of R_p-R5a but produced no detectable changes for S_p-R5a, R_p-R5, and S_p-R5. MD simulations suggested that hydrophobic interactions of the label with the dT_8 C5-methyl group and variations in the occupancy of label conformers that form these interactions, which account qualitatively for the observed EPR spectral changes. This demonstrates a synergistic interplay of experimental and computational approaches, with EPR measurements providing a critical validation of MD simulations, and the MD simulations revealing the molecular characteristics of the system and directing further experimental investigations (e.g., sequence changes). We note that in addition to the R5/R5a probes, a number of nitroxides have been reported to produce variable cw-EPR spectra depending on sequence and secondary structure of DNA and RNA.[38−45] However, to connect the observed spectral features to molecular details at the nitroxide attachment site has been challenging. While MD simulations have been applied to investigate spin-labeled biomolecules,[30,46−56] the combined EPR-mutagenesis-MD approach reported here could broadly aid further development and application of SDSL.

The results reported here also revealed issues that remain to be addressed in investigations of interactions between nitroxide labels and DNA. Specifically, force-field issues and ergodicity are always of concern in MD simulations. The force-field parameters used here have previously given results consistent with experimentally measured internitroxide distances,[30] and the label parameters have also been used independently by other groups.[55,56] However, there were relatively large variations in torsion angle distributions between the 10 ns traces (Tables 1 and S2 and S3 in the Supporting Information), indicating that convergence may not have been established. This hampers in-depth analyses, such as computing transition rates between label conformers and order parameters for a given ensemble, which are required for quantitative correlations with cw-EPR spectra. We note that new parameter sets for similar spin labels[57,58] and improved DNA parametrizations[36,59] have been proposed, particularly for longer (microsecond) simulations, and work has been reported on generating a full EPR spectrum based on MD trajectories, particularly taking advantage of advances in simulation techniques.[46−51] Thus, further improvement and extension of MD simulations may ultimately allow computation of R5/R5a spectra for direct comparison with experimental data.

Modulation of R5a/R5 Motions by DNA. It has been hypothesized that site- and stereospecific behavior of R5 and R5a mainly arise from DNA sequence-dependent variations of (i) sterically allowable rotamer space, (ii) contacts/interactions between DNA and the pyrroline ring, and (iii) local DNA dynamics (flexibility).[21,22] The results reported here provided details to validate this proposed framework, as well as revealing further complexity.

Regarding sterically allowable rotamers, MD simulations clearly demonstrated that steric exclusion from the DNA is a dominant factor that dictates the label behavior. For example, for R_p-R5, while *g*+, *t*, and *g*− conformations are accessible to both t1 and t2, certain t1, t2 combinations (for example, *g*+, *g*+; *g*+, *g*−; and *g*−, *g*+) have <1% occupancy (Table S5 in the Supporting Information), since they position the pyrroline ring within the steric volume of the DNA. In addition, when the DNA backbone at $dG_{6\text{-}pS}dC_7$ adopts a B_I conformation, the t1 *g*+ conformer is hardly occupied for R_p-R5a or R_p-R5 (Tables 2 and S4 and S5 and Figure S1 in the Supporting Information) because of severe clashes between the pyrroline ring and the dG_6 sugar.

dx.doi.org/10.1021/jp303303v | J. Phys. Chem. B 2012, 116, 6387−6396

In terms of contacts/interactions between the DNA and the pyrroline ring, simulations reveal that certain conformers of R_p labels (e.g., t1 $g+$) position the dT_8 C5-methyl group within close proximity to the pyrroline ring and ring methyl groups, indicating probable hydrophobic contacts. For R_p-R5a, the 4-Br atom may further strengthen this label/DNA interaction, while at the same time increasing the fraction of these interaction-capable conformers by reducing the total number of allowed label conformers (Tables 2 and S4 in the Supporting Information). This qualitatively accounts for the spectral differences between R_p-R5a-dT_8 and R_p-R5a-dU_8 (Figures 2 and 3). On the other hand, the absence of 4-Br in R_p-R5 reduces the percentage of interaction-enabled conformers and eliminates interactions between the DNA and the label C4 functionality (Tables 2 and S5 in the Supporting Information), resulting in a lack of detectable spectral changes between R_p-R5-dT_8 and R_p-R5-dU_8 (Figure 2).

Last but not least, a connection between EPR detected R5/R5a motions to local nanosecond DNA backbone dynamics is demonstrated by the covariation of the $dG_{6\text{-}pS}dC_7$ B_{II} and R5/R5a t1 $g+$ conformations (Table 2 and Figures 6 and S1 in the Supporting Information). In previous studies, B_I to B_{II} transitions in DNA duplexes have been reported to occur on a nanosecond time scale in a sequence-dependent manner, with the dG−dC dinucleotide step favoring substantial occupancy of the B_{II} conformation.[34−37] The naturally occurring nanosecond B_I/B_{II} transition at $dG_{6\text{-}pS}dC_7$ results in expanded sterically allowable rotamer space for the labels, allowing additional DNA-nitroxide contacts that influence nitroxide motions to an extent detectable by cw-EPR (i.e., R_p-R5a-dT_8 vs R_p-R5-dU_8). In future studies, it should be very interesting to examine effects on R5/R5a motions from other modes of DNA motions (e.g., sugar puckering, base breathing).

Implications for Use of R5a/R5 to Probe Dynamics and Conformations of Nucleic Acids. Understanding of sequence-dependent coupling between DNA and R5/R5a will significantly improve our ability to extract information from these probes. For instance, spectral sensitivity of R_p-R5a to the dT → dU mutation may be further explored to probe sequence-dependent B_I/B_{II} transition, which may play a role in protein/DNA recognition.[37,60−63] Interestingly, NMR[37] and MD[36] studies on B_I/B_{II} distributions for all 16 dinucleotide steps have revealed an asymmetric preference for B_{II} within dinucleotide base-pair units (e.g., a difference between G_pA and T_pC[37]). These findings draw a parallel with asymmetric R5a/R5 EPR lineshapes previously obtained within dinucleotide base-pair units.[21,22] This provides additional support to a link between DNA local backbone motion and R5a/R5 behavior.

Information on coupling between DNA and R5/R5a will also improve modeling of allowable nitroxide conformers and enable more accurate interpretation of internitroxide distances. We have developed an algorithm, referred to as NASNOX,[19,30] for rapid computation of inter-R5 distances in a DNA[20] or RNA structure.[23] This algorithm depends on the prediction of the conformational distribution of each label. From a computational perspective, MD simulations demand signficant computer resources and are difficult to apply for direct computation of multiple sets of interlabel distances.[30] Therefore, we envision a strategy in which the details of the label conformational distribution obtained from MD simulations of model systems are incorporated empirically in a simple conformer search model, thus enabling efficient and accurate calculations of interlabel distances in the context of determination of nucleic acid folds.

We note that computational approaches, including MD simulations, have been an important tool in characterizing sequence-dependent conformational and dynamic heterogeneity of free DNA duplexes,[36,64−67] but experimental validation of conclusions drawn from these analyses remains challenging. The combined experimental (EPR spectroscopy, DNA mutagenesis) and computational (MD simulations) approach reported in this work paves the way for an in-depth understanding of the behavior of R5a/R5 at a given DNA microenvironment. This is a key step forward toward the use of R5a/R5 to examine intrinsic sequence-dependent conformational and dynamic heterogeneity in large biologically relevant DNA molecules under physiological conditions.

■ ASSOCIATED CONTENT

Supporting Information

Tables S1−S6 and Figures S1 and S2. This material is available free of charge via the Internet at http://pubs.acs.org.

■ AUTHOR INFORMATION

Corresponding Author

*Tel: 213-821-2461. Fax: 213-740-0930. E-mail: pzq@usc.edu (P.Z.Q.). Tel: 323-442-3310. Fax: 323-442-1390. E-mail: ihaworth@usc.edu (I.H.).

Present Addresses

[#]Department of Molecular Biology, The Scripps Research Institute, La Jolla, California 92037, United States.

[▽]Department of Physiology, University of Arizona, Tucson, Arizona 85724, United States.

Author Contributions

[⊥]These authors contributed equally to the manuscript.

Notes

The authors declare no competing financial interest.

■ ACKNOWLEDGMENTS

We gratefully acknowledge support from the NIH (GM069557, P.Z.Q.), NSF (MCB 054652, P.Z.Q.), and a fellowship from Hashemite University (Jordan) to M.H. We thank Dr. Kálmán Hideg (University of Pécs, Pécs, Hungary) for providing reactive precursors of the R5 and R5a probes. Computation for the work described in this paper was supported by the University of Southern California Center for High-Performance Computing and Communications (www.usc.edu/hpcc).

■ REFERENCES

(1) Lawson, C. L.; Berman, H. M. Indirect Readout of DNA Sequence by Proteins. In *Protein-Nucleic Acid Interactions*; Correll, C. C., Rice, P. A., Eds.; Royal Society of Chemistry: Cambridge, 2008; p 66.

(2) Rohs, R.; West, S. M.; Liu, P.; Honig, B. *Curr. Opin. Struct. Biol.* **2009**, *19*, 171.

(3) Rohs, R.; Jin, X.; West, S. M.; Joshi, R.; Honig, B.; Mann, R. S. *Annu. Rev. Biochem.* **2010**, *79*, 233.

(4) Egli, M.; Pallan, P. S. *Curr. Opin. Struct. Biol.* **2010**, *20*, 262.

(5) Segal, E.; Fondufe-Mittendorf, Y.; Chen, L.; Thastrom, A.; Field, Y.; Moore, I. K.; Wang, J. P.; Widom, J. *Nature* **2006**, *442*, 772.

(6) Peckham, H. E.; Thurman, R. E.; Fu, Y.; Stamatoyannopoulos, J. A.; Noble, W. S.; Struhl, K.; Weng, Z. *Genome Res.* **2007**, *17*, 1170.

(7) Rohs, R.; West, S. M.; Sosinsky, A.; Liu, P.; Mann, R. S.; Honig, B. *Nature* **2009**, *461*, 1248.

(8) Hubbell, W. L.; Cafiso, D. S.; Altenbach, C. *Nat. Struct. Biol.* **2000**, *7*, 735.

(9) Fajer, P. G. Electron spin resonance spectroscopy labeling in proteins and peptides analysis. In *Encyclopedia of Analytical Chemistry*; Meyers, R., Ed.; John Wiley & Sons: Chichester, 2000; p 5725.
(10) Klug, C. S.; Feix, J. B. *Methods Cell Biol.* **2008**, *84*, 617.
(11) Sowa, G. Z.; Qin, P. Z. Site-directed spin labeling studies on nucleic acid structure and dynamics. *Progress in Nucleic Acids Research and Molecular Biology*; Academic Press: New York, NY, **2008**; Vol. *82*, p 147.
(12) Robinson, B. H.; Mailer, C.; Drobny, G. *Annu. Rev. Biophys. Biomol. Struct.* **1997**, *26*, 629.
(13) Keyes, R. S.; Bobst, A. M. Spin-labeled nucleic acids. In *Biological Magnetic Resonance*; Berliner, L. J., Ed.; Plenum Press: New York, 1998; Vol. *14*; p 283.
(14) Krstić, I.; Endeward, B.; Margraf, D.; Marko, A.; Prisner, T. Structure and Dynamics of Nucleic Acids. In *EPR Spectroscopy, Applications in Chemistry and Biology*; Drescher, M., Jeschke, G., Eds.; Springer: Berlin/Heidelberg, 2011; Vol. *321*; p 159.
(15) Reginsson, G. W.; Schiemann, O. *Biochem. Soc. Trans.* **2011**, *39*, 128.
(16) Sigurdsson, S. T. *Pure Appl. Chem.* **2011**, *83*, 677.
(17) Nguyen, P.; Qin, P. Z. *WIREs: RNA* **2012**, *3*, 62.
(18) Qin, P. Z.; Butcher, S. E.; Feigon, J.; Hubbell, W. L. *Biochemistry* **2001**, *40*, 6929.
(19) Qin, P. Z.; Haworth, I. S.; Cai, Q.; Kusnetzow, A. K.; Grant, G. P. G.; Price, E. A.; Sowa, G. Z.; Popova, A.; Herreros, B.; He, H. *Nat. Protoc.* **2007**, *2*, 2354.
(20) Cai, Q.; Kusnetzow, A. K.; Hubbell, W. L.; Haworth, I. S.; Gacho, G. P. C.; Van Eps, N.; Hideg, K.; Chambers, E. J.; Qin, P. Z. *Nucleic Acids Res.* **2006**, *34*, 4722.
(21) Popova, A. M.; Kálai, T.; Hideg, K.; Qin, P. Z. *Biochemistry* **2009**, *48*, 8540.
(22) Popova, A. M.; Qin, P. Z. *Biophys. J.* **2010**, *99*, 2180.
(23) Cai, Q.; Kusnetzow, A. K.; Hideg, K.; Price, E. A.; Haworth, I. S.; Qin, P. Z. *Biophys. J.* **2007**, *93*, 2110.
(24) Grant, G. P. G.; Boyd, N.; Herschlag, D.; Qin, P. Z. *J. Am. Chem. Soc.* **2009**, *131*, 3136.
(25) Zhang, X.; Tung, C.-S.; Sowa, G. Z.; Hatmal, M. M.; Haworth, I. S.; Qin, P. Z. *J. Am. Chem. Soc.* **2012**, *134*, 2644.
(26) Grant, G. P. G.; Popova, A.; Qin, P. Z. *Biochem. Biophys. Res. Commun.* **2008**, *371*, 451.
(27) Earle, K. A.; Budil, D. E. Calculating Slow-motion ESR Spectra of Spin-Labeled Polymers. In *Advanced ESR Methods in Polymer Reaserch*; Schlick, S., Ed.; John Wiley and Sons: New York, 2006; p 53.
(28) Meirovitch, E.; Nayeem, A.; Freed, J. H. *J. Phys. Chem. B* **1984**, *88*, 3454.
(29) Leporc, S.; Mauffret, O.; Tevanian, G.; Lescot, E.; Monnot, M.; Fermandjian, S. *Nucleic Acids Res.* **1999**, *27*, 4759.
(30) Price, E. A.; Sutch, B. T.; Cai, Q.; Qin, P. Z.; Haworth, I. S. *Biopolymers* **2007**, *87*, 40.
(31) Wang, J.; Wolf, R. M.; Caldwell, J. W.; Kollman, P. A.; Case, D. A. *J. Comput. Chem.* **2004**, *25*, 1157.
(32) Darden, T.; York, D.; Pedersen, L. *J. Chem. Phys.* **1993**, *98*, 10089.
(33) Lavery, R.; Sklenar, H. *J. Biomol. Struct. Dyn.* **1988**, *6*, 63.
(34) Hartmann, B.; Piazzola, D.; Lavery, R. *Nucleic Acids Res.* **1993**, *21*, 561.
(35) Perez, A.; Luque, F. J.; Orozco, M. *J. Am. Chem. Soc.* **2007**, *129*, 14739.
(36) Lavery, R.; Zakrzewska, K.; Beveridge, D.; Bishop, T. C.; Case, D. A.; Cheatham, T., 3rd; Dixit, S.; Jayaram, B.; Lankas, F.; Laughton, C.; Maddocks, J. H.; Michon, A.; Osman, R.; Orozco, M.; Perez, A.; Singh, T.; Spackova, N.; Sponer, J. *Nucleic Acids Res.* **2010**, *38*, 299.
(37) Heddi, B.; Oguey, C.; Lavelle, C.; Foloppe, N.; Hartmann, B. *Nucleic Acids Res.* **2010**, *38*, 1034.
(38) Okonogi, T. M.; Alley, S. C.; Reese, A. W.; Hopkins, P. B.; Robinson, B. H. *Biophys. J.* **2000**, *78*, 2560.
(39) Edwards, T. E.; Okonogi, T. M.; Robinson, B. H.; Sigurdsson, S. T. *J. Am. Chem. Soc.* **2001**, *123*, 1527.
(40) Gannett, P. M.; Darian, E.; Powell, J.; Johnson, E. M.; Mundoma, C.; Greenbaum, N. L.; Ramsey, C. M.; Dalal, N. S.; Budil, D. E. *Nucleic Acids Res.* **2002**, *30*, 5328.
(41) Cekan, P.; Jonsson, E. O.; Sigurdsson, S. T. *Nucleic Acids Res.* **2009**, *37*, 3990.
(42) Cekan, P.; Sigurdsson, S. T. *J. Am. Chem. Soc.* **2009**, *131*, 18054.
(43) Smith, A. L.; Cekan, P.; Brewood, G. P.; Okonogi, T. M.; Alemayehu, S.; Hustedt, E. J.; Benight, A. S.; Sigurdsson, S. T.; Robinson, B. H. *J. Phys. Chem. B* **2009**, *113*, 2664.
(44) Krstic, I.; Frolow, O.; Sezer, D.; Endeward, B.; Weigand, J. E.; Suess, B.; Engels, J. W.; Prisner, T. F. *J. Am. Chem. Soc.* **2010**, *132*, 1454.
(45) Shelke, S. A.; Sigurdsson, S. T. *Nucleic Acids Res.* **2012**, *40*, 3732.
(46) Robinson, B. H.; Slusky, L. J.; Auteri, F. P. *J. Chem. Phys.* **1992**, *96*, 2609.
(47) Stoica, I. *J. Phys. Chem. B* **2003**, *108*, 1771.
(48) Beier, C.; Steinhoff, H.-J. *Biophys. J.* **2006**, *91*, 2647.
(49) Budil, D. E.; Sale, K. L.; Khairy, K. A.; Fajer, P. G. *J. Phys. Chem. A* **2006**, *110*, 3703.
(50) DeSensi, S. C.; Rangel, D. P.; Beth, A. H.; Lybrand, T. P.; Hustedt, E. J. *Biophys. J.* **2008**, *94*, 3798.
(51) Sezer, D.; Freed, J. H.; Roux, B. *J. Am. Chem. Soc.* **2009**, *131*, 2597.
(52) Sale, K.; Song, L.; Liu, Y. S.; Perozo, E.; Fajer, P. *J. Am. Chem. Soc.* **2005**, *127*, 9334.
(53) Fajer, M. I.; Li, H.; Yang, W.; Fajer, P. G. *J. Am. Chem. Soc.* **2007**, *129*, 13840.
(54) Piton, N.; Mu, Y.; Stock, G.; Prisner, T. F.; Schiemann, O.; Engels, J. W. *Nucleic Acids Res.* **2007**, *35*, 3128.
(55) Ding, F.; Layten, M.; Simmerling, C. *J. Am. Chem. Soc.* **2008**, *130*, 7184.
(56) Galiano, L.; Ding, F.; Veloro, A. M.; Blackburn, M. E.; Simmerling, C.; Fanucci, G. E. *J. Am. Chem. Soc.* **2009**, *131*, 430.
(57) Houriez, C. l.; FerreÌ, N.; Siri, D.; Masella, M. *J. Phys. Chem. B* **2009**, *113*, 15047.
(58) Stendardo, E.; Pedone, A.; Cimino, P.; Cristina Menziani, M.; Crescenzi, O.; Barone, V. *Phys. Chem. Chem. Phys.* **2010**, *12*, 11697.
(59) Perez, A.; Marchan, I.; Svozil, D.; Sponer, J.; Cheatham, T. E., 3rd; Laughton, C. A.; Orozco, M. *Biophys. J.* **2007**, *92*, 3817.
(60) Wecker, K.; Bonnet, M. C.; Meurs, E. F.; Delepierre, M. *Nucleic Acids Res.* **2002**, *30*, 4452.
(61) Heddi, B.; Foloppe, N.; Bouchemal, N.; Hantz, E.; Hartmann, B. *J .Am. Chem. Soc.* **2006**, *128*, 9170.
(62) Rene, B.; Masliah, G.; Antri, S. E.; Fermandjian, S.; Mauffret, O. *J. Phys. Chem. B* **2007**, *111*, 4235.
(63) Tian, Y.; Kayatta, M.; Shultis, K.; Gonzalez, A.; Mueller, L. J.; Hatcher, M. E. *J. Phys. Chem. B* **2009**, *113*, 2596.
(64) Olson, W. K.; Gorin, A. A.; Lu, X. J.; Hock, L. M.; Zhurkin, V. B. *Proc. Natl. Acad. Sci. U.S.A.* **1998**, *95*, 11163.
(65) Lankas, F.; Sponer, J.; Langowski, J.; Cheatham, T. E., 3rd. *Biophys. J.* **2003**, *85*, 2872.
(66) Fujii, S.; Kono, H.; Takenaka, S.; Go, N.; Sarai, A. *Nucleic Acids Res.* **2007**, *35*, 6063.
(67) Goni, J. R.; Perez, A.; Torrents, D.; Orozco, M. *Genome Biol.* **2007**, *8*, R263.